System-environmental entanglement in critical spin systems under ZZ-decoherence and its relation to strong and weak symmetries

Yoshihito Kuno[1⋆], Takahiro Orito[2] and Ikuo Ichinose[3†]

1 Graduate School of Engineering science, Akita University, Akita 010-8502, Japan
2 Institute for Solid State Physics, The University of Tokyo, Kashiwa, Chiba, 277-8581, Japan
3 Department of Applied Physics, Nagoya Institute of Technology, Nagoya, 466-8555, Japan

⋆ kuno421yk@gmail.com

Abstract

Open quantum many-body systems exhibit nontrivial behavior under decoherence. In particular, system-environmental entanglement (SEE) is one of the efficient quantities for classifying mixed states subject to decoherence. In this work, we investigate the SEE of critical spin chains under nearest-neighbor ZZ-decoherence. We numerically show that the SEE exhibits a specific scaling law, in particular, its system-size-independent term (“g-function”) changes drastically its behavior in the vicinity of phase transition caused by decoherence. For the XXZ model in its gapless regime, a transition diagnosed by strong Rényi-2 correlations occurs as the strength of the decoherence increases. We determine the location of the phase transition by investigating the g-function that exhibits a sharp change in the critical region of the transition. Furthermore, we find that the value of the SEE is twice that of the system under single-site Z-decoherence, which was recently studied by conformal field theory. From the viewpoint of Rényi-2 Shannon entropy, which is closely related to the SEE at the maximal decoherence, we clarify the origin of this g-function behavior.

Received Date
Accepted Date
Published Date

Contents

---

1 Introduction

In practical systems, pure quantum states are exposed by environment, and emergent decoherence produces inevitable physical effects on the pure state. In most of studies searching novel quantum many-body states, it is assumed that the many-body system is isolated and is not affected by environment. However, in research field such as quantum computers and quantum memories, effect of interactions with environment, especially decoherence [1], is an important research subject. For quantum devises such as quantum memory [2–5] and noisy-intermediate-scale quantum computer [2, 6, 7], decoherence from environment generates undesired effects on the manipulation of quantum information.

On the other hand, interplay between environment and quantum many-body system can lead to nontrivial quantum phase transition and critical phenomena with physical properties, which are not observed in isolated quantum systems.

Recently, mixed states having no pure-state counterparts in their physical properties attract lots of attention. As an example, topologically-ordered states as well as symmetry protected topological pure states [8, 9] change to nontrivial mixed states with another type of topological property through interactions with environment [10–17]. Furthermore, recent studies are discussing and clarifying symmetries of the mixed state and their spontaneous symmetry breaking (SSB) emerging from decoherence.

There are various types of SSBs in the mixed state, such as strong symmetry SSB, weak symmetry SSB, strong-to-weak SSB (SWSSB) and strong-to-trivial SSB, etc, [11, 12, 18–28], and some of mixed states have a nontrivial long-range order (LRO). Discovering novel types of SSBs as well as a measure for observing them is an on-going important issue in quantum information and condensed matter communities.

In particular, some critical quantum states under decoherence are an interesting playground to investigate mixed state quantum phase transition and its criticality. As concrete examples, the recent works [29, 30] studied mixed state phase transitions in critical spin chains by the conformal field theory (CFT), which are induced by local on-site decoherence. In Refs. [29, 30], system-environmental entanglement (SEE) was observed and analytically examined to find that SEE exhibits an interesting scaling law having universal term independent of the system size called "g-function" [31]. This universal term characterizes infra-red properties of mixed states.

In this work, instead of on-site decoherence, we shall study effects of a multi-sites decoherence of ZZ-type on critical states in the transverse-field Ising model (TFIM) and XXZ model. These states are described by $c = 1/2$ and $c = 1$ CFTs, respectively. The previous studies showed that this type of decoherence can induce nontrivial LROs and long-range entanglement for mixed states, e.g., SWSSB states [11,12,18–28].

In this setup, we study the following issues:

1. For critical ground states of the TFIM and XXZ models, is ZZ-decoherence relevant? In particular, we are interested in how the decoherence transfers the initial critical state into a critical mixed state and if nontrivial behavior of SEE emerges there.

2. If mixed state in the above models changes non-trivially under ZZ-decoherence, does the SEE exhibit the scaling law proposed in the previous works, $S_{SE} = \alpha L - s_0 + \mathcal{O}(L^{-1})$ [29,30]? If this scaling law holds, how the universal term s_0 (characterizing low-energy property of the system) differs from that of the system under the on-site decoherence studied in [29,30]? If there is difference, what is the origin for that?

3. Is there any relationship in behavior between the g-function and a symmetry order parameter of emerging mixed states? In particular, how a measure of entanglement and symmetry order parameters are related with each other?

To answer the above questions, we employ the doubled Hilbert space formalism [32,33] and filtering methods [34,35] in addition to numerical approach by using matrix product state (MPS). In this numerical approach, the SEE is efficiently calculated from the norm of the filtered MPS defined on ladder spin systems. By using the numerical approach, we find that ZZ-decoherence for the critical states in both the critical TFIM and XXZ models induces novel critical mixed phases with strong Rényi-2 correlation, and that the SEE exhibits the scaling law expected in [29,30,36]. However, interestingly enough, the universal term of the SEE (or g-function) takes different values from that of the single-site decoherence considered in [30,36].

For the critical TFIM case, we numerically observe that the SEE exhibits the expected scaling law, and the value of the g-function under the maximal decoherence is related to the value obtained from the Rényi-2 Shannon entropy [37,38].

As a more interesting result, we numerically show that for the critical XXZ model, the g-function for the strong ZZ-decohered mixed state is twice that of the system under a local on-site Z-decoherence [30]. We analytically explain the origin of this behavior of the g-function by considering the decoherence limit and using the Rényi-2 Shannon entropy.

The rest of this paper is organized as follows. In Sec. 2, we introduce two critical spin-1/2 systems and ZZ-decoherence as channel applied to the critical states of the models. In Sec. 3, the SEE is introduced, which is one of target physical quantities in this work. In Sec. 4, we explain the doubled Hilbert space formalism to investigate the critical states subject to decoherence. There, the decoherence can be regarded as the filtering operation to the doubled critical states defined on the ladder spin system, which is explained somewhat in detail. In Sec. 5, we perform the systematic numerical calculations by using the MPS and the filtering method for both the TFIM and XXZ models. Some correlation functions [19,20,39] to observe the strong or weak symmetry SSB are introduced and numerically calculated. Simultaneously, the SEE is investigated. In particular, the universal g-function denoted by e^{s_0} is extensively studied. In Sec. 6, we discuss physical meaning of the universal scaling law and the g-function e^{s_0} in the SEE obtained numerically. Section 7 is devoted to summery and conclusion.

2 Critical system and decoherence

In this work, we study effects of decoherence applied to critical states of two 1D spin systems, represented by Pauli operators X_j, Y_j and Z_j. The first system is the 1D TFIM, Hamiltonian of which is given by

$$H_{\mathrm{TFI}} = -\sum_{j=0}^{L-1}\Big[Z_j Z_{j+1} + X_j\Big],$$

and the second one is the 1D XXZ model, which is given by

$$H_{\mathrm{XXZ}} = \sum_{j=0}^{L-1}\Big[X_j X_{j+1} + Y_j Y_{j+1} + \Delta Z_j Z_{j+1}\Big],$$

where Δ is anisotropic parameter. Throughout this work, periodic boundary conditions are imposed. Both models possess Z_2 symmetry, which is nothing but a global spin flip $U_X = \prod_{j=0}^{L-1} X_j$. For the model H_{XXZ}, the critical ground state appears for $|\Delta| < 1$ described by Tomonaga-Luttinger Liquid (TLL) with its TLL parameter $K = \frac{\pi}{2(\pi - \arccos\Delta)}$, where $K > 1/2$. It is known that the critical ground states in the above models are described by $c = 1/2$ and $c = 1$ CFTs, respectively [40].

In this work, we study effects of system-environment interactions, in particular, ZZ-decoherence applied to the critical state $\rho = |\phi_0\rangle\langle\phi_0|$, where $|\phi_0\rangle$ stands for the pure ground state at criticality in the TFIM or XXZ model. This kind of decoherence is induced by the interactions between the system and environment such as, $\rho_{\mathrm{SE}} = \hat{U}(\rho \otimes \rho_{\mathrm{E}})\hat{U}^{\dagger}$, where ρ_{E} is density matrix of environment and $\hat{U}$ is the unitary operator representing the interactions between the system and environment. After tracing out the degrees of freedom of environment, we obtain the system density matrix subject to the resultant decoherence.

Description of this decoherence by channel is given by [41]

$$\mathcal{E}^{ZZ}_{tot}[\rho] = \left(\prod_{j=0}^{L-1} \mathcal{E}^{ZZ}_j\right)[\rho] \equiv \rho_D, \tag{1}$$

$$\mathcal{E}^{ZZ}_j[\rho] \equiv (1-p_{zz})\rho + p_{zz} Z_j Z_{j+1} \rho Z_{j+1} Z_j, \tag{2}$$

where the strength of the decoherence is tuned by p_{zz} (j-independent), and $0 \leq p_{zz} \leq 1/2$. Decoherence phase transition of the mixed state ρ_D is a target of the present study.

For $p_{zz} = 1/2$, the channel corresponds to the projective measurement of $Z_j Z_{j+1}$ for a link between j- and $j+1$-th sites without monitoring outcomes, which is called maximal decoherence. As we explained in the introduction, the reason why we consider ZZ-decoherence is that it can give an insight into how system-environment entanglement and strong/weak U_X symmetry of the system [42] are related with each other [1]. Besides the SEE, we are also interested in how the above mentioned symmetries of non-trivial mixed states emerge as the strength of the decoherence is increased.

3 System-environmental entanglement

This study focuses on the SEE for a density matrix ρ [29, 30] given by

$$S_{SE} = -\log \mathrm{Tr}[\rho^2]. \tag{3}$$

This is also called the second-order Rényi entropy for the density matrix ρ. The SEE captures the degree of mixing of non-trivial mixed states induced by decoherences [29], and also it

[1] The detail of the definition of the strong and weak symmetries as for the U_X-symmetry is discussed in Appendix in [39].

can be diagnostic for mixed-state phase transitions. As another useful quantity, we consider Rényi-2 Shannon entropy (SE) [37,38] given by

$$S_S \;=\; -\log\Big[\sum_{\ell} p_\ell^2\Big] \quad \text{with } p_\ell = |\langle e_\ell|\phi_0\rangle|^2, \tag{4}$$

where the set $\{|e_\ell\rangle\}$ is a properly chosen basis set of state for 2^L-sites spin-1/2 system. In the maximal decoherence limit $p_{zz} \to 1/2$, the above S_{SE} can have a close relationship with S_S calculated with a set of Z-basis for $\{|e_\ell\rangle\}$ as $\mathcal{E}_j^{ZZ}[\rho]$ in that limit is nothing but the projection operator on Z-domain wall states. (See Sec. VI for more details.) This fact will be utilized later on for the analysis of the numerical results.

We expect that the SEE exhibits the following system-size scaling as in the previous works [29,30],

$$S_{SE}(L, p_{zz}) = \alpha_L L - s_0 + \mathcal{O}(L^{-1}), \tag{5}$$

where α_L is a non-universal coefficient depending on ultra-violet cutoff. On the other hand, s_0 is a universal quantity that is independent of the system size and also ultra-violet setups, and its value is believed to be related to the low-energy properties of the system [30,31,36,37]. The physical quantity s_0 can quantitatively capture the change in entanglement structure and the change of the mixed state, such as emergence of strong or weak SSB. The scaling law of Eq. (5) can be also applied to the SE (S_S) for the critical ground state $|\phi_0\rangle$, and by setting the basis $\{|e_\ell\rangle\}$ to a set of local product states, S_S corresponds to the half-cylinder "entanglement entropy" of 2D quantum Rokhsar-Kivelson (pure) wave function. There, the value of s_0 characterizes the (low-energy) long-range properties for the quantum state [36].

If $s_0 \neq 0$ for $\mathcal{E}(\rho_0)$ where ρ_0 is a pure state, the decoherence channel $\mathcal{E}[\cdot]$ is an infra-red relevant operator in the sense of renormalization group [29,30]. In general, e^{s_0} decreases if the boundary perturbation is relevant, known as "g-theorem" [31]. However, recent study [30] showed that such a decreasing behavior does not necessarily hold due to dangerously-irrelevant decoherence effect [30,43].

4 Doubled Hilbert space formalism

To investigate the effect of ZZ-decoherence $\mathcal{E}_{tot}^{ZZ}$ to the critical ground states, we employ the doubled Hilbert space formalism [32,33] and filtering methods [34,35]. We shall explain these formalisms in this section.

We first consider the pure density matrix of the critical ground state of H_{TFI} or H_{XXZ}, $\rho_0 = |\phi_0\rangle\langle\phi_0|$, and denote the original Hilbert space of the spin-1/2 system by $\mathcal{H}$. For the analysis of the decohered state ρ_D through the channel $\mathcal{E}_{tot}^{ZZ}$, the doubled Hilbert space is introduced [44] as $\mathcal{H}_u \otimes \mathcal{H}_\ell$, where the subscripts u and ℓ refer to the upper and lower Hilbert spaces corresponding to ket and bra states of mixed state density matrix, respectively. Under vectorization formula (followed by [44]) for a density matrix ρ [32,33], $\rho \longrightarrow |\rho\rangle\rangle \equiv \frac{1}{\sqrt{\dim[\rho]}} \sum_k |k^*\rangle \otimes \rho |k\rangle$, where $\{|k\rangle\}$ is an orthonormal set of states in the Hilbert space $\mathcal{H}$ and $|\rho\rangle\rangle$ resides on the doubled Hilbert space $\mathcal{H}_u \otimes \mathcal{H}_\ell$. In particular for pure state $|\phi_0\rangle$, $|\rho_0\rangle\rangle$ is given by $|\rho_0\rangle\rangle \equiv |\phi_0^*\rangle|\phi_0\rangle$, where the asterisk denotes the complex conjugation.

In this formalism, decoherence channel $\mathcal{E}[\cdot]$ is mapped to operator $\hat{\mathcal{E}}$ acting on the state vector $|\rho\rangle\rangle$ in the doubled Hilbert space $\mathcal{H}_u \otimes \mathcal{H}_\ell$ [18,44] and denoted as $\hat{\mathcal{E}}|\rho\rangle\rangle$. Then, the decoherence channel $\mathcal{E}^{ZZ}_{tot}$ is expressed as the follows,

$$\begin{aligned}\hat{\mathcal{E}}^{ZZ}_{tot}(p_{zz}) &= \prod_{j=0}^{L-1}\Big[(1-p_{zz})\hat{I}^{*}_{j,u}\otimes\hat{I}_{j,\ell}+p_{zz}Z^{*}_{j,u}Z^{*}_{j+1,u}\otimes Z_{j,\ell}Z_{j+1,\ell}\Big]\\ &= \prod_{j=0}^{L-1}(1-2p_{zz})^{1/2}e^{\tau_{zz}Z_{j,u}Z_{j+1,u}\otimes Z_{j,\ell}Z_{j+1,\ell}},\end{aligned} \tag{6}$$

where $\hat{I}_{j,u(\ell)}$ is an identity operator for site-j vector space in $\mathcal{H}_{u(\ell)}$, $Z(X)_{j,u(\ell)}$ is Pauli-$Z(X)$ operator at site j in the space $\mathcal{H}_{u(\ell)}$ and $\tau_{zz}=\tanh^{-1}[p_{zz}/(1-p_{zz})]$. The application of the channel operator $\hat{\mathcal{E}}^{ZZ}_{tot}(p_{zz})$ changes the initial state $|\rho_0\rangle\rangle$ and also the norm of the vector $|\rho_0\rangle\rangle$. In this sense, the operation $\hat{\mathcal{E}}^{ZZ}_{tot}(p_{zz})$ is non-unitary. Here, note that the initial doubled state $|\rho_0\rangle\rangle$ is nothing but the ground state of the two decoupled TFIM or XXZ model on a *two-leg spin-1/2 ladder* with the Hilbert space $\mathcal{H}_u\otimes\mathcal{H}_\ell$ and the Hamiltonian $H^{u}_{\mathrm{TFI(XXZ)}}+H^{\ell}_{\mathrm{TFI(XXZ)}}$ on the upper and lower chains.

In the ladder system, the decohered state $|\rho_D\rangle\rangle$ is given as

$$|\rho_D\rangle\rangle\equiv\hat{\mathcal{E}}^{ZZ}_{tot}|\rho_0\rangle\rangle=C(p_{zz},L)\prod_{j=0}^{L-1}\Big[e^{\tau_{zz}\hat{h}^{zz}_{j,j+1}}\Big]|\rho_0\rangle\rangle, \tag{7}$$

where the operators $\hat{h}^{zz}_{j,j+1}=Z_{j,u}Z_{j+1,u}\otimes Z_{j,\ell}Z_{j+1,\ell}$ and $C(p_{zz},L)\equiv(1-2p_{zz})^{L/2}$. The filtering is the application of the operator $\hat{\mathcal{E}}^{ZZ}_{tot}$ to the state $|\rho_0\rangle\rangle$. This operation can be regarded as non-unitary imaginary-time evolution where the time interval is $\tau_{zz}(p_{zz})$. We investigate the properties of the mixed ρ_D by studying its counterpart $|\rho_D\rangle\rangle$. In particular, since the norm $\langle\langle\rho_D|\rho_D\rangle\rangle$ corresponds to the purity $\mathrm{Tr}[\rho_D^2]$ (>0), the SEE, which is one of the target quantities in this work, is given by the logarithm of the norm [30]

$$S_{SE}(p_{zz},L)=-\log\langle\langle\rho_D|\rho_D\rangle\rangle. \tag{8}$$

Before numerically observing the effect of ZZ-decoherence on the critical ground states, we expect that for small p_{zz}, ZZ-decoherence is irrelevant and the initial critical properties are preserved, whereas for $p_{zz}\to 1/2$ $(\lambda_{zz}\to\infty)$, the decoherence $ZZZZ$ effect gives a significant impact to the ground states: The decohered mixed states can have a long-range order (LRO) such as Z_2 SWSSB, which is a main subject of the present study. At least, such a state with a LRO is definitely different from the initial critical state $|\rho_0\rangle\rangle$. We later verify this expectation by observing the SEE and other physical quantities.

5 Numerical analysis of system environmental entanglement

We numerically study the decohered state $|\rho_D\rangle\rangle$ by using the MPS to analyze large systems and to calculate SEE and some correlators characterizing orders such as SWSSB emerging in the decohered state vector $|\rho_D\rangle\rangle$. We prepare the initial critical state $|\rho_0\rangle\rangle$ by using DMRG in the TeNPy package [45, 46]. The filtering operation $\hat{\mathcal{E}}^{ZZ}_{tot}(p_{zz})$ in Eq. (6) applied to the MPS $|\rho_0\rangle\rangle$ can be efficiently carried out by making use of the libraries in TeNPy [45, 46].

In addition to SEE, we also introduce the (reduced) susceptibility of Rényi-2 correlator to corroborate the observation of the properties of the mixed state ρ_D. The susceptibility is given by

$$\chi^{\mathrm{II}}_{ZZ} = \frac{2}{L}\sum_{r=1}^{L/2}C^{\mathrm{II}}_{ZZ}(0,r),$$

where C^{II}_{ZZ} is the Rényi-2 correlator for the state $|\rho_D\rangle\rangle$,

$$C^{\mathrm{II}}_{ZZ}(i,j) \equiv \frac{\langle\langle \rho_D | Z_{i,u} Z_{j,u} Z_{i,\ell} Z_{j,\ell} | \rho_D \rangle\rangle}{\langle\langle \rho_D | \rho_D \rangle\rangle}.$$

In the original 1D system, a counterpart of $C^{\mathrm{II}}_{ZZ}(i,j)$ is given by

$$C^{\mathrm{II}}_{ZZ}(i,j) \equiv \frac{\mathrm{Tr}[Z_i Z_j \rho_D Z_j Z_i \rho_D]}{\mathrm{Tr}[(\rho_D)^2]}.$$

This observable provides us an order parameter for detecting both the LRO and SSB of the strong symmetry, but *not* those of the weak symmetry [18–20, 47]. Note that this quantity $C^{\mathrm{II}}_{ZZ}(i,j)$ exhibits non-trivial behavior in the whole parameter region, that is, it varies concomitantly with the decoherence nature of the state.

In general, one can consider another quantity, the canonical correlation function given by

$$C^{\mathrm{I}}_{Z}(i,j) = \mathrm{Tr}[\rho_D Z_i Z_j] = \frac{\langle\langle \mathbf{1} | Z_{i,u} Z_{j,u} | \rho_D \rangle\rangle}{\langle\langle \mathbf{1} | \rho_D \rangle\rangle},$$

where $|\mathbf{1}\rangle\rangle \equiv \frac{1}{2^{3L/2}} \prod_{j=0}^{L-1} |t\rangle_j$ with $|t\rangle_j = |\uparrow_u \uparrow_\ell\rangle_j + |\downarrow_u \downarrow_\ell\rangle_j$. The observable $C^{\mathrm{I}}_{Z}(i,j)$ can be an order parameter characterizing the genuine SSB (i.e., weak symmetry SSB) [18–20]. However, in our target system subject to the ZZ decoherence, this quantity is invariant under the decoherence since $\mathrm{Tr}[\rho_D Z_i Z_j] = \mathrm{Tr}[\mathcal{E}^{ZZ}_{tot}(\rho_0) Z_i Z_j] = \mathrm{Tr}[\rho_0 Z_i Z_j]$, and $C^{\mathrm{I}}_{Z}(i,j)$ keeps the value of the pure critical state of ρ_0 for any p_{zz}. Thus, $|C^{\mathrm{I}}_{Z}(i,j)|$ has a power law decay, $\propto \frac{1}{|i-j|^\eta}$ as a function of $|i-j|$. The power law decay corresponds to that of $c = 1/2$ and $c = 1$ CFT for the TFIM and XXZ model, respectively.

Before showing the numerical calculations, we discuss the diagnosis of non-trivial mixed states from the view point of the above two quantities, $C^{\mathrm{II}}_{ZZ}(i,j)$ and $|C^{\mathrm{I}}_{Z}(i,j)|$.

The combination of $C^{\mathrm{II}}_{ZZ}(i,j)$ and $|C^{\mathrm{I}}_{Z}(i,j)|$ can detect various symmetry breaking phases including the SWSSB, which is recently proposed in Refs. [18–20]. In the system with the strong Z_2 symmetry [2], if a state exhibits $C^{\mathrm{II}}_{ZZ}(i,j) \sim \mathcal{O}(1)$ and $|C^{\mathrm{I}}_{Z}(i,j)| \sim 0$ for $|i-j| \to \infty$, SSB of the off-diagonal (i.e., strong) symmetry occurs and the diagonal (i.e., weak) symmetry is preserved [18]. This is SWSSB. Also if $C^{\mathrm{II}}_{ZZ}(i,j) \sim \mathcal{O}(1)$ and $|C^{\mathrm{I}}_{Z}(i,j)| \sim \mathcal{O}(1)$, then both the weak and strong SSBs occur called strong-to-trivial SSB. [If reader is interested in brief explanation of strong and weak symmetries as well as their combination of SSB and the notion of SWSSB, see [16, 39].]

Since $|C^{\mathrm{I}}_{Z}(i,j)|$ of the systems exhibits the power-law decay for any decoherence strength, $|C^{\mathrm{I}}_{Z}(i,j)| \sim 0$ for $|i-j| \to \infty$ limit, the target mixed state exhibits the SWSSB or remains symmetric as decoherence is getting strong.

5.1 Numerical results for critical TFIM

We numerically observe effects of ZZ-decoherence on the critical state of the TFIM. First, calculations of the observables χ^{II}_{ZZ} is shown in Fig. 1. As shown in Fig. 1 (a), χ^{II}_{ZZ} increases with p_{zz} and saturates to unity for large p_{zz}. We observe the existence of the plateau regime with $\chi^{\mathrm{II}}_{ZZ} = 1$ for $p_{zz} \gtrsim 0.4$, without system size dependence, while for $p_{zz} \lesssim 0.3$, small system size dependence appears, where the value decreases as increasing system size L. In particular, for the limit $p_{zz} = 0$, we carefully verified that χ^{II}_{ZZ} exhibits a power-law-decreasing behavior

[2] Strictly, to define the SWSSB, we require that the initial state, target, decoherence channel, and final decohered state satisfy to be strongly-symmetric for a target on-site symmetry [19, 20].

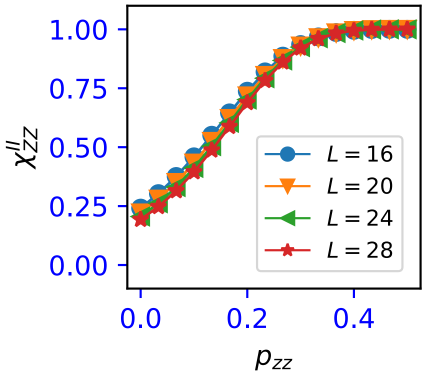

Figure 1: Behaviors of χ^{II}_{ZZ} for TFIM critical states under ZZ-decoherence. Data for various system sizes are displayed, indicating negligibly small system-size dependence.

with respect to L [not shown] and its power exponent is fairly close to the value predicted by the conventional correlation function of the critical ground state of the TFIM, and for $L \to \infty$, χ^{II}_{ZZ} smoothly approaches zero with that exponent. This behavior implies that in our finite size numerics, a sharp phase transition does not occur and the state smoothly approaches the unique state for $p_{zz} \to 1/2$.

As mentioned in the previous section, $|C^{\mathrm{I}}_Z(i,j)| \sim 0$ for $|i-j| \to \infty$, the numerical result indicates that the state for $p_{zz} > 0.4$ is in a SWSSB phase. That is, large ZZ-decoherence induces the transfer of the system from the symmetric phase to the SWSSB phase, although a clear phase transition point cannot be identified.

We next focus on the SEE. Here, we observe how g-function e^{s_0}, extracted from the various system size data, behaves as p_{zz} increases. The detail of the practical procedure and an concrete fitting example are shown in Appendix A. Results are shown in Fig. 2, and we find that the SEE is well-fitted by the scaling law Eq. (5). As shown in Fig. 2 (a), the g-function e^{s_0} increases slightly with p_{zz}. We further observe that the different system size data do not cross with each other, and then, e^{s_0} does not indicate the existence of a phase transition induced by the ZZ-decoherence. Combined with the results of χ^{II}_{ZZ}, the ZZ-decoherence simply induces a crossover from the critical state of the TFIM to the mixed state with critical properties. Furthermore, interestingly enough, Fig. 2 (b) shows that the values of s_0 at $p_{zz} = 1/2$ (the exponent of the extracted g-function) for the various system sizes are very close to the value obtained from the universal constant $\gamma_{n=2} = \log 2$ in the SE measured by the single-site Z-basis [38], as $-\gamma_{n=2} + \log 2 = 0$. In order to verify this observation, we perform the extrapolation of s_0 for $L_{sd} \to \infty$, and find that s_0 approaches zero as observed in Fig. 2 (c). Detailed discussion on this point, especially the reason why the obtained s_0 takes $-\gamma_{n=2} + \log 2 = 0$, is given later on.

In Appendix C, we show how the critical ground state of the TFIM evolves under $X + ZZ$-decoherence. In the previous paper [39], we investigated this system from view point of SWSSB, and obtained interesting results showing the existence of a phase transition at a finite strength of decoherence. Numerical results of the g-function in Appendix C exhibit a similar phase transition behavior. Then, an important and interesting question is how these two observables relate with each other. This issue is discussed in detail in subsequent sections for the XXZ model, which exhibits similar behaviors with the TFIM under the $X + ZZ$-decoherence.

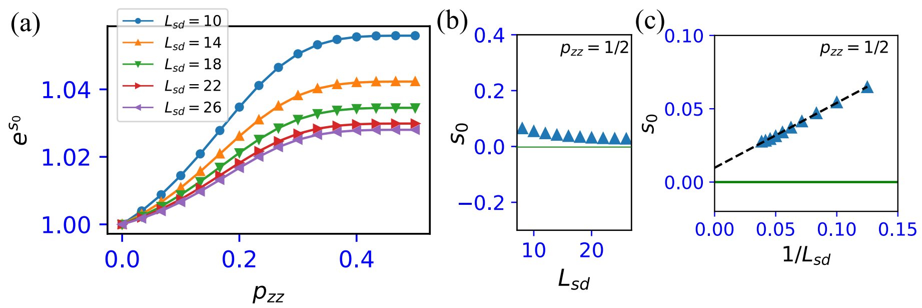

Figure 2: (a)p_{zz}-dependence of the g-function e^{s_0} for various sets of system size $\{L_{sd}, L_{sd}+2, L_{sd}+4, L_{sd}+6\}$ for critical TFIM. (b) L_{sd}-dependence of the extracted value of s_0 for $p_{zz} = 1/2$. The green line, $-\gamma_{n=2} + \log 2 = -\log 2 + \log 2 = 0$, where $\gamma_{n=2}$ is the estimation value of the subleading term of the Rényi-2 Shannon entropy in the previous work [37, 38], the value of which is $\gamma_{n=2} = \log 2$ [38]. The values of s_0 was extracted by the numerical fitting procedure by using the set of four different system sizes, $\{L_{sd}, L_{sd}+2, L_{sd}+4, L_{sd}+6\}$. (c) The extrapolation of s_0 for $p_{zz} = 1/2$ in $L_{sd} \to \infty$. The linear fitting function is estimated as $s_0 = -0.44(1/L_{sd}) + 0.01$.

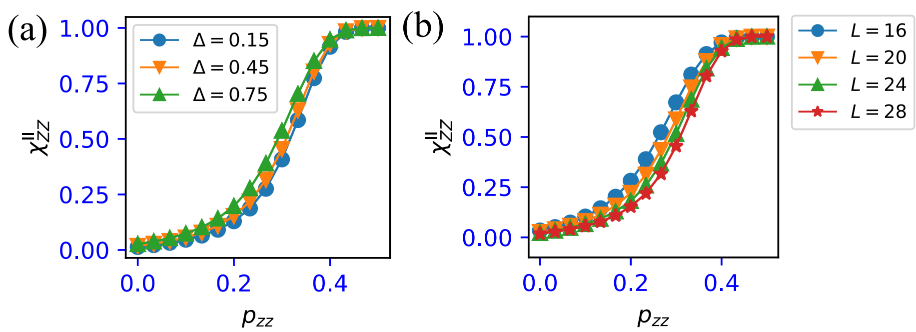

Figure 3: (a) Behaviors of χ^{II}_{ZZ} for XXZ critical states under ZZ-decoherence. (b) System size dependence of χ^{II}_{ZZ} for $\Delta = 0.45$. We set $L = 28$ (total 56 sites).

5.2 Numerical results for critical XXZ model

We turn to the numerical study on the critical ground state of the XXZ model. The p_{zz}-dependence of χ^{II}_{ZZ} for various values of Δ (in the TLL regime) is shown in Figs. 3 (a). As seen in Fig. 3 (a), χ^{II}_{ZZ} increases with p_{zz} and saturates for large p_{zz}, that is, the plateau regime with $\chi^{\mathrm{II}}_{ZZ} = 1$ emerges in $p_{zz} \gtrsim 0.4$. We further observe the system size dependence with Δ fixed as shown in Fig. 3 (b). The small but finite system size dependence of χ^{II}_{ZZ} exists in the intermediate p_{zz} regime, but for $p_{zz} \gtrsim 0.4$, χ^{II}_{ZZ} has a finite value without system size dependence. As mentioned in the previous section, $|C^{\mathrm{I}}_Z(i,j)|$ exhibits power law decay as a function of the distance $|i-j|$ and $|C^{\mathrm{I}}_Z(i,j)| \sim 0$ for $|i-j| \to \infty$. Thus, for $p_{zz} \gtrsim 0.4$ regime, the SWSSB mixed phase is expected to emerge for any value of Δ. Here, we ask if there exists a sharp phase transition to the SWSSB state. While estimation of critical decoherence to the SWSSB is not so easily from the data of χ^{II}_{ZZ}, its existence is not denied from the calculation of g-function in Fig. 4 as we discuss below.

Next, we move on to the calculation of the SEE. Here, we observe how g-function e^{s_0}, extracted from the various system size data, behaves in the region where the mixed state

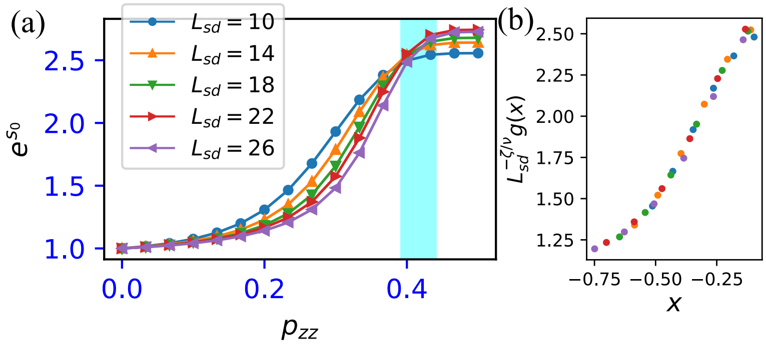

Figure 4: (a) p_{zz}-dependence of the g-function e^{s_0} for various sets of system size $\{L_{sd}, L_{sd}+2, L_{sd}+4, L_{sd}+6\}$ for critical XXZ model. The values of s_0 was extracted by the numerical fitting procedure by using the set of four different system size, $\{L_{sd}, L_{sd}+2, L_{sd}+4, L_{sd}+6\}$. We set $\Delta = 0.45$. (b) Scaling data collapse, where the label $x = (p_{zz} - p^c_{zz})L_{sd}^{1/\nu}$. We used data points within $0.2 \leq p_{zz} \leq 0.5$. We estimated $p_c = 0.439(0)$ with $\zeta = 0.007(3)$ and $\nu = 2.519(8)$.

changes into the SWSSB stat as p_{zz} increases.

We calculate the SEE and confirm that the SEE is well-fitted by the scaling law of Eq. (5) and extract the g-function. Then, we observe the g-function for $\Delta = 0.45$ varying the system size. The results are displayed in Fig. 4 (a). The g-function e^{s_0} increases as p_{zz} increases, and we find that all system-size data lines cross with each other at $p_{zz} \sim 0.4$. This value of p_{zz} coincides with the saturation point of χ^{II}_{ZZ} in Fig. 3(a). This behavior is observed for other Δ's, as shown in Appendix B. This crossing of the data indicates the existence of the phase transition between critical and the mixed state with strong Rényi-2 correlation.

To elucidate the properties of the transition, we perform a finite-size scaling analysis for the g-function by employing the most general form of scaling ansatz,

$$e^{s_0} = L_{sd}^{\zeta/\nu} g((p_{zz} - p^c_{zz})L_{sd}^{1/\nu}),$$

where p^c_{zz} is the critical transition point and ζ and ν are critical exponents. The scaling analysis was carried out with the help of pyfssa [48, 49]. The result is shown in Fig. 4(b), where the clear data collapse is observed, supporting the genuine phase transition. There, we estimate $p^c_{zz} = 0.439(0)$ with $\zeta = 0.007(3)$ and $\nu = 2.519(8)$. The value of ζ is close to zero similarly to the scaling-analysis result performed in the previous works [29, 36]. These numerical results indicate the existence of the phase transition between the critical XXZ state and the mixed state with strong Rényi-2 correlation(SWSSB) [3].

Next, we show the most interesting numerical results in this work. We observe Δ-dependence of the g-function for $p_{zz} = \frac{1}{2}$. The results are displayed in Fig. 5. Surprisingly enough, we find the value of e^{s_0} is very close to $2\sqrt{2K}$, where the value of $\sqrt{2K}$ was estimated by analytical methods and verified numerically in the previous study on the XXZ chain *under single-site Z-decoherence* [30]. This multiple factor "2" discrepancy can be related to the long-range nature of the Rényi-2 correlation in the decohered mixed state. In the thermodynamic limit, the Z_2

[3] Obviously whether this transition observed by the spin correlations and that of system-environment entanglement observed by e^{s0} take place simultaneously is an interesting question. A plausible possibility is that there exists a single phase transition between the critical state and decohereded mixed state, but different observables exhibit its signal at different values of p_{zz}. Typical example is the KT transition of the 2D classical XY spin model, where the specific heat and corelation functions give different values of the transition [50]. For the present systems, it is a future problem.

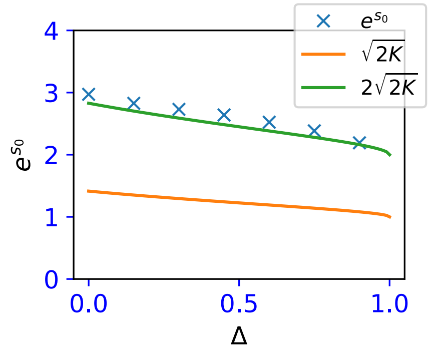

Figure 5: Δ-dependence of g-function e^{s_0} for $p_{zz} = 1/2$ limit. The values of s_0 for each Δ were extracted by the numerical fitting procedure for the set of the different system sizes $L = 12, 16, 20, 24, 28$ data. The orange and green lines are $e^{s_0} = \sqrt{2K(\Delta)}$ and $e^{s_0} = 2\sqrt{2K(\Delta)}$, respectively.

strong symmetry is spontaneously broken and it is realized in the ensemble level. However in the finite system, a GHZ (cat) state emerges respecting the Z_2 strong symmetry, and this long-range entanglement can be the origin of the multiple factor "2".

We also find that the origin of the multiple factor "2" is understood by analytically observing the connection of Rényi-2 Shannon entropy for $p_{zz} = 1/2$ limit. The numerical assisted analytical understanding is shown in the following section. By this observation, it is clarified that emergence of the GHZ state is an essential ingredient of this phenomenon.

In addition as we stated briefly in the above, we numerically investigate effects of another decoherence for the critical state of the TFIM, and we find that the g-function behaves nontrivially for strong decoherence. This result is shown in Appendix B.

6 Analysis of universal s_0 for $p_{zz} = 1/2$ limit

In the previous section, we numerically observed the universal term s_0. The values of e^{s_0} change from one to nontrivial values for both critical spin systems. In particular for the decoherence limit $p_{zz} = 1/2$, we found that the values of e^{s_0} are related to the previously studied ones in [30, 36]. In this section, we discuss this relationship by analytically studying the connection between the SEE for ρ_D with $p_{zz} = 1/2$ limit and the Rényi-2 Shannon entropy for the glassy GHZ basis. Numerical study is also used to corroborate the observation.

6.1 Glassy GHZ expansion of ρ_D for $p_{zz} = 1/2$ decohered limit

We first prove that the decohered state ρ_D for $p_{zz} = 1/2$ limit (projective ZZ-measurement limit) can be expanded by the glassy GHZ states, that is, we find the following representation: For $p_{zz} = 1/2$ ZZ-decoherence limit, the state ρ_D is expanded as

$$\mathcal{E}^{ZZ}_{tot}[\rho_0]_{p_{zz}=1/2} \quad = \quad \sum_{g,\alpha=\pm} P^{(g,\alpha)} \rho_0 P^{(g,\alpha)}, \tag{9}$$

where $P^{(g,\alpha)} = |g^\alpha\rangle\langle g^\alpha|$, and $\{|g^\alpha\rangle\}$ are a set of the glassy GHZ states of L-site spin system. The glassy GHZ basis is labeled by the number $g = 0, 1, \cdots, 2^{L-1} - 1$ and α labels the parity

for the global spin flip $\mathbf{Z}_2$ operator U_X and $U_X|g^{\pm}\rangle = \pm|g^{\pm}\rangle$.
For example, $|g^{\pm}=1^{\pm}\rangle = \frac{1}{\sqrt{2}}[|\uparrow\downarrow\uparrow\cdots\uparrow\rangle \pm |\downarrow\uparrow\downarrow\cdots\downarrow\rangle]$.

Here, we comment that Eq. (9) is satisfied for any ρ_0 if ρ_0 is an eigenstate of U_X, that is, ρ_0 is given as $\rho_0 = |\phi_0\rangle\langle\phi_0|$ and $|\phi_0\rangle$ is symmetric under U_X in the present case.

We shall prove Eq. (9) in the following way;
First, $\mathcal{E}^{ZZ}_{tot}[\rho]_{p_{zz}=1/2}(\equiv \rho_{D,p_{zz}=1/2})$ can be rewritten as

$$\rho_{D,p_{zz}=1/2} = \sum_{\vec{\beta}}\Big(P^{ZZ,\beta_{L-1}}_{L-1}P^{ZZ,\beta_{L-2}}_{L-2}\cdots P^{ZZ,\beta_1}_{1}P^{ZZ,\beta_0}_{0}\Big)\rho_0\Big(P^{ZZ,\beta_0}_{0}P^{ZZ,\beta_1}_{1}\cdots P^{ZZ,\beta_{L-2}}_{L-2}P^{ZZ,\beta_{L-1}}_{L-1}\Big), \tag{10}$$

where P^{ZZ,β_j}_j is the projection operator defined by $P^{ZZ,\beta_j}_j = \frac{1+\beta_j Z_j Z_{j+1}}{2}$ with the outcome β_j taking ± 1, and $\vec{\beta} = \{\beta_0, \beta_1, \cdots, \beta_{L-2}, \beta_{L-1}\}$. Note that there is a crucial constraint for the outcome, that is, β_{L-1} is fixed by the patterns of $\{\beta_0, \beta_1, \cdots, \beta_{L-2}\}$, $\beta_{L-1} = \prod_{j=0}^{L-2}\beta_j$, coming from the constraint for ZZ-measurement operator, $\prod_{j=0}^{L-1} Z_j Z_{j+1} = 1$. The sum $\sum_{\vec{\beta}}$ in Eq. (10), therefore, means the summation of total 2^{L-1} outcome patterns of $\{\beta_0, \beta_1, \cdots, \beta_{L-2}\}$.

By making use of the identity $1 = \sum_c |c\rangle\langle c|$, where $|c\rangle$ is a L-site basis state of the local spin Z_j such as $|\uparrow\uparrow\uparrow\cdots\uparrow\rangle$ ($\sum_c$ means all sum of product Z basis pattern.), Eq. (10) can be expressed as,

$$\begin{aligned}
[\text{Eq. (10)}] &= \sum_{\vec{\beta}}\Big(P^{ZZ,\beta_{L-1}}_{L-1}P^{ZZ,\beta_{L-2}}_{L-2}\cdots P^{ZZ,\beta_1}_{1}P^{ZZ,\beta_0}_{0}\Big)\Big[\sum_c |c\rangle\langle c|\Big]\rho_0\Big[\sum_c |c\rangle\langle c|\Big]\\
&\quad\times\Big(P^{ZZ,\beta_0}_{0}P^{ZZ,\beta_1}_{1}\cdots P^{ZZ,\beta_{L-2}}_{L-2}P^{ZZ,\beta_{L-1}}_{L-1}\Big)\\
&= \sum_{c-\{\bar{c}\}}\Big[|c\rangle\langle c| + |\bar{c}\rangle\langle\bar{c}|\Big]\rho_0\Big[|c\rangle\langle c| + |\bar{c}\rangle\langle\bar{c}|\Big]\\
&= \sum_{c-\{\bar{c}\}}\Big[K_c\rho_0K_c + K_c\rho_0N_c + N_c\rho_0K_c + N_c\rho_0N_c\Big],
\end{aligned} \tag{11}$$

where we have introduced projective operators defined as $K_c = |c\rangle\langle c|$ and $N_c = |\bar{c}\rangle\langle\bar{c}|$, and note that $|c\rangle$ and $|\bar{c}\rangle$ are a "parity pair" given by $|c\rangle = U_X|\bar{c}\rangle$. The sum $\sum_{c-\{\bar{c}\}}$ denotes the summation over the subset of basis $\{|c\rangle\}$ (the total element of the subset is 2^{L-1}), that is, each elements of which are not connected by the parity U_X.

On the other hand, we note that since the glassy GHZ basis can be written by $|g^{\pm}\rangle = \dfrac{1}{\sqrt{2}}[|c\rangle \pm |\bar{c}\rangle]$, the RHS of Eq. (9) can be expanded as

$$\begin{aligned}
[\text{RHS of Eq. (9)}] &= \sum_{c-\{\bar{c}\}}\frac{1}{2}\Big[K_c\rho_0K_c + K_c\rho_0N_c + L_c\rho_0L_c + L_c\rho_0M_c\\
&\quad + M_c\rho_0L_c + M_c\rho_0M_c + N_c\rho_0K_c + N_c\rho_0N_c\Big],
\end{aligned} \tag{12}$$

where $L_c = |c\rangle\langle\bar{c}|$ and $M_c = |\bar{c}\rangle\langle c|$.

Then, if the state ρ_0 is unique critical ground state of the target Hamiltonian, $U_X|\phi_0\rangle = \pm|\phi_0\rangle$ since U_X commutes with the Hamiltonian and $(U_X)^2 = 1$. This fact directly leads to

$$\langle c|\phi_0\rangle = \pm\langle\bar{c}|\phi_0\rangle. \tag{13}$$

By substituting the above relation into Eq. (12), we verify that Eq. (12) is equal to Eq. (11), regardless of the sign on the RHS of Eq. (13). Thus, Eq. (9) has been proved.

In general, the sigh of Eq.(13) can depend on the system size, boundary conditions and the model parameters. To further validate the above argument, the sigh of Eq.(13) is observed for practical cases by using the exact diagonalization to find that the following relations hold for the critical states in both the TFIM and XXZ models,

$$\langle c|\phi_0\rangle = \pm\langle\bar{c}|\phi_0\rangle \text{ for XXZ critical,} \tag{14}$$
$$\langle c|\phi_0\rangle = \langle\bar{c}|\phi_0\rangle \text{ for TFIM critical.} \tag{15}$$

Here, we comment that for the above XXZ case, numerically, the sign depends only on the system size and there is no Δ-dependence.

6.2 SEE-SE correspondence for ZZ-projective measurement limit

Equation (9) gives an important relation: the SEE for $\rho_{D,p_{zz}=1/2}$ denoted by $S_{SE,p_{zz}=1/2}$ is written as

$$S_{SE,p_{zz}=1/2} = -\log \mathrm{Tr}[\rho^2_{D,p_{zz}=1/2}] \overset{\text{Eq.(9)}}{=} -\log\Big[\sum_{g,\alpha=\pm} |\langle g^\alpha|\phi_0\rangle|^4\Big]. \tag{16}$$

The last quantity in Eq. (16) can be regarded as the Rényi-2 Shannon entropy S_S [37,38] of the critical state $|\phi_0\rangle$ *in terms of the glassy GHZ basis* $\{|g^\alpha\rangle\}$.

As a result, we find that the SEE of the mixed state ρ_D for $p_{zz}=1/2$ limit corresponds to the Rényi-2 Shannon entropy. This observation sheds light on the results of s_0 and its g-function e^{s_0} obtained in the previous section, as we explain in the following subsection.

6.3 Relation between SEE of Z-decoherence limit and SEE of ZZ-decoherence limit

We further find an interesting relation between the SEE for $p_{zz}=1/2$ limit $S_{SE,p_{zz}=1/2}$ and the Rényi-2 Shannon entropy of the critical state $|\phi_0\rangle$ in terms of Z-product basis. This corresponds to the case, in which on-site local maximal Z_j-decoherence is applied to the critical state $|\phi_0\rangle$ at all system sites, previously studied in [30,36]. In this case,

$$\begin{aligned}\mathrm{Tr}[\rho^2_{D,p_{zz}=1/2}] &= \mathrm{Tr}\Big[\sum_{c-\{\bar{c}\}}(K_c\rho_0K_c\rho_0K_c + K_c\rho_0L_c\rho_0K_c + L_c\rho_0K_c\rho_0L_c + L_c\rho_0L_c\rho_0L_c)\Big]\\ &= \sum_c |\langle c|\rho_0|c\rangle|^2 + \sum_c |\langle c|\rho_0|\bar{c}\rangle|^2.\end{aligned} \tag{17}$$

Then, by using the numerical observation of Eq. (14) or Eq. (15), we easily obtain

$$\mathrm{Tr}[\rho^2_{D,p_{zz}=1/2}] = 2\sum_c |\langle c|\rho_0|c\rangle|^2. \tag{18}$$

The above equation leads to the following relation

$$S_{SE,p_{zz}=1/2} = -\log\Big[\mathrm{Tr}[\rho^2_{D,p_{zz}=1/2}]\Big] = -\log\Big[2\sum_c |\langle c|\rho_0|c\rangle|^2\Big] = S_S(\{|c\rangle\}) - \log 2. \tag{19}$$

That is, the SEE for $p_{zz}=1/2$ limit relates to the Rényi-2 Shannon entropy of the critical state $|\phi_0\rangle$ in terms of Z-product basis (denoted by $S_S(\{|c\rangle\})$) with the deviation "*minus* $\log 2$".

Then, since the Rényi-2 Shannon entropy of the critical state $|\phi_0\rangle$ in terms of Z-product basis $S_S(\{|c\rangle\})$ corresponds to the SEE for the critical state under the on-site local Z_j-decoherence limit [30], denoted by $S^Z_{SE,p_z=1/2}$. Thus, $S_{SE,p_{zz}=1/2}$ relates to $S^Z_{SE,p_z=1/2}$ with the deviation "*minus* $\log 2$", where the precise form of $S^Z_{SE,p_z=1/2}$ is already known [30,37,38].

Finally, we get a scaling law of $S_{SE,p_{zz}=1/2}$ and its universal term s_0 for both TFIM and XXZ models by making use of the previous studies [30,37,38], in which the scaling law of $S^{Z}_{SE,p_z=1/2}$ and values of the universal term s_0 are already obtained as $S^{Z}_{SE,p_z=1/2}=\alpha_1^{\mathrm{TFIM(XXZ)}}L - s_0^{\mathrm{TFIM(XXZ)}}+\mathcal{O}(L^{-1})$. Then, $S_{SE,p_{zz}=1/2}$ has the following forms:

$$S_{SE,p_{zz}=1/2}=\begin{cases}\alpha_1^{\mathrm{TFIM}}L-(s_0^{\mathrm{TFIM}}+\log 2)+\mathcal{O}(L^{-1}) & \text{for TFIM critical}\\ \alpha_1^{\mathrm{XXZ}}L-(s_0^{\mathrm{XXZ}}+\log 2)+\mathcal{O}(L^{-1}) & \text{for XXZ critical,}\end{cases}$$

where $\alpha_1^{\mathrm{TFI(XXZ)}}$ are non-universal coefficients. Also, it is known that $s_0^{\mathrm{TFIM}}=-\log 2$ [37,38]. The g-function of the universal parts for $S_{SE,p_{zz}=1/2}$, e^{s_0} are regarded as

$$e^{s_0}=\begin{cases}e^0 & \text{for TFIM and from the result in [37,38]}\\ 2\sqrt{2K} & \text{for XXZ and from the result in [30].}\end{cases} \tag{20}$$

In particular we find that the g-function e^{s_0} of $S_{SE,p_{zz}=1/2}$ for the critical XXZ model has a multiple factor "2" compared to the g-function e^{s_0} of $S^{Z}_{SE,p_z=1/2}$ in Ref. [30], which is consistent to the result in Fig. 5.

Then, the numerical results of the g-function for $p_{zz}=1/2$ limit of the critical TFIM shown in Fig. 2 are consistent with the TFIM result of Eq. (20).

7 Conclusion

This work studied the effects of the ZZ-decoherence acting on the critical states for both the TFIM and XXZ models. By making use of the DMRG and filtering methods, we investigated how the SEE behaves and how criticality changes by the effects of the decoherence. For both the TFIM and XXZ models, we numerically found that the SEE exhibits the scaling law $\alpha L - s_0+\mathcal{O}(L^{-1})$ for any strength of the ZZ-decoherence, and that the g-function, e^{s_0}, changes its value as varying the strength of decoherence. Simultaneously, the decoherence induces the change in the mixed states where a long-range ordered state appears as observed by the the Rényi-2 correlator. The ZZ-decoherence induces a drastic change of the mixed state in the XXZ model, whereas for the critical TFIM, it does not.

For the g-function, we found that: (I) For the TFIM, the value of the e^{s_0} continuously changes and approaches unity (s_0 approach zero) as increasing the decoherence. We numerically demonstrated that the estimated value $s_0=0$ for $p_{zz}=1/2$ limit is related to the subleading term of the Rényi-2 Shannon entropy in the previous work [37,38]. (II) The case of the XXZ model has rich physical phenomena. In particular, the value of e^{s_0} for the critical XXZ model under strong ZZ-decoherence is twice that of the previous study on Z-decoherence obtained by the CFT and RG analysis [30]. Our numerical findings of the value of e^{s_0} were analytically understood. For the $p_{zz}=1/2$ limit, the SEE in our system corresponds to the Rényi-2 Shannon entropy for the glassy GHZ set of basis, value of which is related to the Rényi-2 Shannon entropy for Z-product basis. Therefore, our numerically estimated e^{s_0}'s are related to the values of e^{s_0} obtained in the previous studies [30,37,38].

As shown in this work, the SEE is a useful measure to characterize and classify mixed state with some orders. The numerical methods that we introduced in this work can be an efficient tool for discovering universality for various critical mixed states under decoherence.

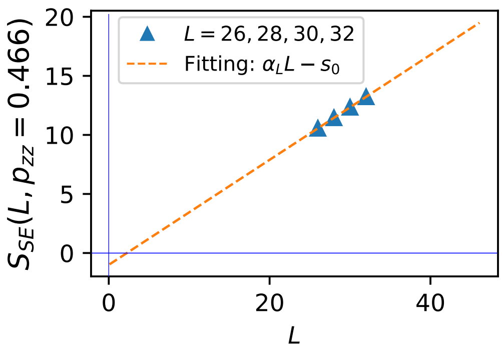

Figure 6: Fitting procedure to extract s_0 from different system size data of S_{EE}. This behavior is in the case of the XXZ model. We set the parameters $p_{zz} = 0.466$, $\Delta = 0.45$ and plot the SEE for various sets of system size $L = 26$, 28, 30 and 32. The estimated value of s_0 is $s_0 = 1.0019$

Acknowledgements

This work is supported by JSPS KAKENHI: JP23K13026(Y.K.) and JP23KJ0360(T.O.).

Author contributions This is optional. If desired, contributions should be succinctly described in a single short paragraph, using author initials.

Funding information Authors are required to provide funding information, including relevant agencies and grant numbers with linked author's initials. Correctly-provided data will be linked to funders listed in the Fundref registry.

A Protocol of determining s_0

We here show how to numerically determine the value of s_0 from the SEE data, S_{SE}. For a fixed p_{zz} and Δ, we calculate S_{SE} for the various system sizes, and then, we plot the L-dependence of S_{SE}. In many cases, the data points exhibit behavior of a linear function of L. Then, we carry out the fitting procedure by assuming the fitting function, $S_{SE}(L, p_{zz}) = \alpha_L L - s_0$. By an optimization method, we can obtain s_0. An concrete example is shown in Fig. 6 corresponding to the data point for $p_{zz} = 0.466$ in Fig. 4 left. Here, four different system-size data exhibit a linear function behavior, then we can easily extract the estimated value of s_0.

B e^{s_0} behavior for different Δ cases in XXZ model

We show the additional results for Fig. 4 left panel. We here plot the different Δ cases in Figs. 7 (a) and 7 (b). The behaviors for both cases are the same with the one shown in Fig. 4 left panel. We also observe that data crossing for the different L_{sd} data line occurs around $p_{zz} = 0.4$, that is, the crossing is independent to the value of Δ. Moreover, for both Δ case shown in in Figs. 7 (a) and 7 (b), in $p_{zz} = 1/2$ limit, the value of e^{s_0} tends to converge as increasing L_{sd}. Thus, for $L_{sd} \to \infty$, a converged value of s_0 exists which is independent of Δ (We assume the regime $|\Delta| < 1$).

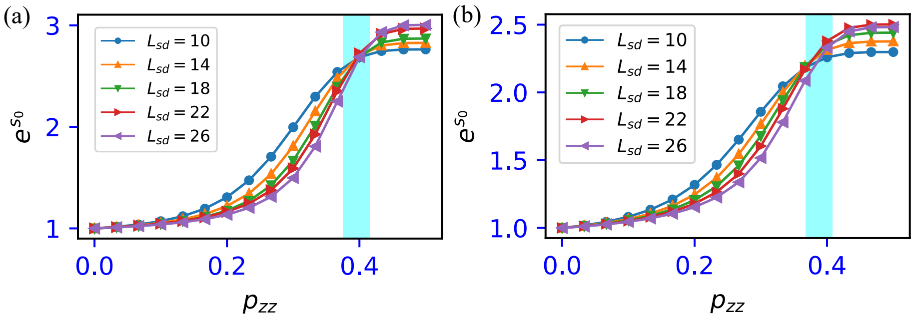

Figure 7: p_{zz}-dependence of the g-function e^{s_0} for various sets of system size $\{L_{sd}, L_{sd}+2, L_{sd}+4, L_{sd}+6\}$ for critical XXZ model. (a) $\Delta = 0.15$ case. (b) $\Delta = 0.75$ case.

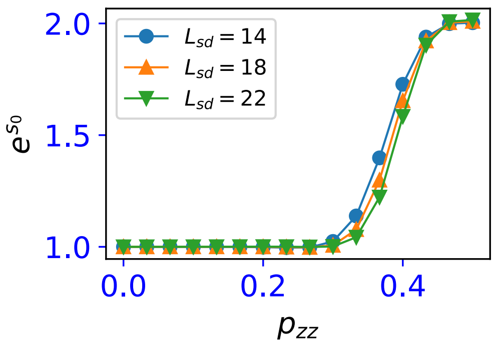

Figure 8: $p_{zz(x)}$-dependence of the g-function e^{s_0} for various sets of system size $\{L_{sd}, L_{sd}+2, L_{sd}+4, L_{sd}+6\}$ for critical TFIM model under $X+ZZ$ decoherence.

C System-environment entanglement in the critical TFIM under $X+ZZ$-decoherence

As another concrete numerical example, we study the effects of the multiple decoherences to the critical state of the TFIM. This setting is considered in the previous study [39]. We consider not only ZZ-decoherence but also a local X-decoherence, the corresponding operator in the doubled Hilbert space formalism is given by

$$\hat{\mathcal{E}}_X(p_x)=\prod_{j=0}^{L-1}\left[(1-p_x)\hat{I}^*_{j,u}\otimes\hat{I}_{j,\ell}+p_xX^*_{j,u}\otimes X_{j,\ell}\right]=\prod_{j=0}^{L-1}(1-2p_x)^{1/2}e^{\tau_x X_{j,u}\otimes X_{j,\ell}}, \tag{C.1}$$

where $\tau_x = \tanh^{-1}[p_x/(1-p_x)]$ and $0 \le p_x \le 1/2$.

We consider the following multiple channel

$$|\rho_D\rangle\rangle \equiv \hat{\mathcal{E}}^{ZZ}_{tot}\hat{\mathcal{E}}_X|\rho_0\rangle\rangle = C(p_{zz},p_x,L)\prod_{j=0}^{L-1}\left[e^{\tau_{zz}\hat{h}^{zz}_{j,j+1}}e^{\tau_x\hat{h}^x_j}\right]|\rho_0\rangle\rangle, \tag{C.2}$$

where $\hat{h}^{zz}_{j,j+1} = Z_{j,u}Z_{j+1,u} \otimes Z_{j,\ell}Z_{j+1,\ell}$, $\hat{h}^{x}_{j} = X_{j,u} \otimes X_{j,\ell}$ and $C(p_{zz}, p_x, L) \equiv (1-2p_{zz})^{L/2}(1-2p_x)^{L/2}$. Then, we expect that our target decohered state $|\rho_D\rangle\rangle$ is closely related to the ground states of the quantum Ashkin-Teller model [51], the Hamiltonian of which is given on the ladder as follows,

$$\begin{aligned} H_{\mathrm{qAT}} &= -\sum_{j=0}^{L-1}[Z_{j,u}Z_{j+1,u} + Z_{j,\ell}Z_{j+1,\ell} + \lambda_{zz}Z_{j,u}Z_{j,\ell}Z_{j+1,u}Z_{j+1,\ell}] \\ &\quad -\sum_{j=0}^{L-1}[X_{j,u} + X_{j,\ell} + \lambda_x X_{j,u}X_{j,\ell}]. \end{aligned} \tag{C.3}$$

The above Hamiltonian is derived from a highly-anisotropic version of 2D classical Ashkin-Teller model [52, 53] by the time-continuum-limit formalism [54], and then the Hamiltonian H_{qAT} has $Z_2 \times Z_2$ symmetry with generators $\prod X_{j,u}$ and $\prod X_{j,\ell}$. Furthermore, there are parameter relations such as $\lambda_{zz} \longleftrightarrow \tau_{zz}(p_{zz})$ and $\lambda_x \longleftrightarrow \tau_x(p_x)$, which are expected to qualitatively hold. The global ground state phase diagram of H_{qAT} has been investigated in detail [51, 55–57]. In particular, there is a critical line in the phase diagram, which is given by $\lambda_{zz} = \lambda_x \equiv \lambda > 0$ (since $\tau_{zz(x)} > 0$) with $-1/\sqrt{2} \leq \lambda \leq 1$, and the criticality is described by the bosonic CFT [40]. Then, for $\lambda > 1$, a diagonal Z_2 symmetric phase appears (called "partially-ordered phase" [51]).

We investigate the mixed state of Eq. (C.2) under the condition of the probabilities $p_{zz} = p_x$ to realize the decoherence corresponding to H_{qAT} with $\lambda_{zz} = \lambda_x (= \lambda)$. Increase of $p_{zz(x)}$ corresponds to an increase of λ in the qAT model.

Based on this setup, we numerically investigate the SEE for the state $|\rho_D\rangle\rangle$ by using the same MPS and filtering method to the main text. We also find that from the calculation of the SEE, the scaling law of Eq. (5) holds, and we extract the g-function e^{s_0} from the data. The result as increasing $p_{zz}(= p_x)$ is shown in Fig. 8. Here, we observe that the g-function increases as p_{zz} increases and we find that the saturation value of the g-function e^{s_0} for $p_{zz} = 1/2$ is exactly $e^{s_0} = 2$, that is, $s_0 = \log 2$. The value of which is reminiscent of an expected value $s_0 = \log d$ with $d = 2$ proposed in [36], where the SE of the two degenerate SSB ground state of the TFIM in terms of Z-product basis and d means the ground state degeneracy of the pure ground state of the TFIM.

References

[1] C. W. Gardiner and P. Zoller, *Quantum Noise*, Springer, second edn. (2000).

[2] J. Preskill, *Quantum computing in the nisq era and beyond*, Quantum **2**, 79 (2018), doi:10.22331/q-2018-08-06-79.

[3] E. Dennis, A. Kitaev, A. Landahl and J. Preskill, *Topological quantum memory*, Journal of Mathematical Physics **43**(9), 4452–4505 (2002), doi:10.1063/1.1499754.

[4] C. Wang, J. Harrington and J. Preskill, *Confinement-higgs transition in a disordered gauge theory and the accuracy threshold for quantum memory*, Annals of Physics **303**(1), 31–58 (2003), doi:10.1016/s0003-4916(02)00019-2.

[5] T. Ohno, G. Arakawa, I. Ichinose and T. Matsui, *Phase structure of the random-plaquette z2 gauge model: accuracy threshold for a toric quantum memory*, Nuclear Physics B **697**(3), 462 (2004), doi:https://doi.org/10.1016/j.nuclphysb.2004.07.003.

[6] S. Ebadi, T. T. Wang, H. Levine, A. Keesling, G. Semeghini, A. Omran, D. Bluvstein, R. Samajdar, H. Pichler, W. W. Ho, S. Choi, S. Sachdev *et al.*, *Quantum phases of matter on a 256-atom programmable quantum simulator*, Nature **595**(7866), 227 (2021), doi:10.1038/s41586-021-03582-4.

[7] D. Bluvstein, S. J. Evered, A. A. Geim, S. H. Li, H. Zhou, T. Manovitz, S. Ebadi, M. Cain, M. Kalinowski, D. Hangleiter, J. P. Bonilla Ataides, N. Maskara *et al.*, *Logical quantum processor based on reconfigurable atom arrays*, Nature **626**(7997), 58 (2024), doi:10.1038/s41586-023-06927-3.

[8] B. Zeng, X. Chen, D.-L. Zhou and X.-G. Wen, *Quantum information meets quantum matter – from quantum entanglement to topological phase in many-body systems*, URL https://arxiv.org/abs/1508.02595 (2018), 1508.02595.

[9] X. Wen, *Quantum Field Theory of Many-body Systems: From the Origin of Sound to an Origin of Light and Electrons*, Oxford graduate texts. Oxford University Press, ISBN 9780191713019 (2004).

[10] Y. Bao, R. Fan, A. Vishwanath and E. Altman, *Mixed-state topological order and the errorfield double formulation of decoherence-induced transitions*, URL https://arxiv.org/abs/2301.05687 (2023), 2301.05687.

[11] Z. Wang, Z. Wu and Z. Wang, *Intrinsic mixed-state topological order*, PRX Quantum **6**, 010314 (2025), doi:10.1103/PRXQuantum.6.010314.

[12] R. Sohal and A. Prem, *Noisy approach to intrinsically mixed-state topological order*, PRX Quantum **6**, 010313 (2025), doi:10.1103/PRXQuantum.6.010313.

[13] C. Zhang, Y. Xu, J.-H. Zhang, C. Xu, Z. Bi and Z.-X. Luo, *Strong-to-weak spontaneous breaking of 1-form symmetry and intrinsically mixed topological order*, Phys. Rev. B **111**, 115137 (2025), doi:10.1103/PhysRevB.111.115137.

[14] S. Sang, Y. Zou and T. H. Hsieh, *Mixed-state quantum phases: Renormalization and quantum error correction*, Phys. Rev. X **14**, 031044 (2024), doi:10.1103/PhysRevX.14.031044.

[15] Y.-H. Chen and T. Grover, *Unconventional topological mixed-state transition and critical phase induced by self-dual coherent errors*, Phys. Rev. B **110**, 125152 (2024), doi:10.1103/PhysRevB.110.125152.

[16] Y. Kuno, T. Orito and I. Ichinose, *Intrinsic mixed-state topological order in a stabilizer system under stochastic decoherence: Strong-to-weak spontaneous symmetry breaking from a percolation point of view*, Phys. Rev. B **111**, 064111 (2025), doi:10.1103/PhysRevB.111.064111.

[17] X.-J. Yu, S. Yang, S. Liu, H.-Q. Lin and S.-K. Jian, *Gapless symmetry-protected topological states in measurement-only circuits*, URL https://arxiv.org/abs/2501.03851 (2025), 2501.03851.

[18] J. Y. Lee, C.-M. Jian and C. Xu, *Quantum criticality under decoherence or weak measurement*, PRX Quantum **4**, 030317 (2023), doi:10.1103/PRXQuantum.4.030317.

[19] L. A. Lessa, R. Ma, J.-H. Zhang, Z. Bi, M. Cheng and C. Wang, *Strong-to-weak spontaneous symmetry breaking in mixed quantum states*, PRX Quantum **6**, 010344 (2025), doi:10.1103/PRXQuantum.6.010344.

[20] P. Sala, S. Gopalakrishnan, M. Oshikawa and Y. You, *Spontaneous strong symmetry breaking in open systems: Purification perspective*, Phys. Rev. B **110**, 155150 (2024), doi:10.1103/PhysRevB.110.155150.

[21] Y. Kuno, T. Orito and I. Ichinose, *Strong-to-weak symmetry breaking states in stochastic dephasing stabilizer circuits*, Phys. Rev. B **110**, 094106 (2024), doi:10.1103/PhysRevB.110.094106.

[22] Z. Liu, L. Chen, Y. Zhang, S. Zhou and P. Zhang, *Diagnosing strong-to-weak symmetry breaking via wightman correlators*, Communications Physics **8**(1), 274 (2025), doi:10.1038/s42005-025-02199-7.

[23] Y. Guo and S. Yang, *Strong-to-weak spontaneous symmetry breaking meets average symmetry-protected topological order*, Phys. Rev. B **111**, L201108 (2025), doi:10.1103/PhysRevB.111.L201108.

[24] J. Shah, C. Fechisin, Y.-X. Wang, J. T. Iosue, J. D. Watson, Y.-Q. Wang, B. Ware, A. V. Gorshkov and C.-J. Lin, *Instability of steady-state mixed-state symmetry-protected topological order to strong-to-weak spontaneous symmetry breaking*, URL https://arxiv.org/abs/2410.12900 (2024), 2410.12900.

[25] Z. Weinstein, *Efficient detection of strong-to-weak spontaneous symmetry breaking via the rényi-1 correlator*, URL https://arxiv.org/abs/2410.23512 (2024), 2410.23512.

[26] T. Ando, S. Ryu and M. Watanabe, *Gauge theory and mixed state criticality*, URL https://arxiv.org/abs/2411.04360 (2024), 2411.04360.

[27] L. Chen, N. Sun and P. Zhang, *Strong-to-weak symmetry breaking and entanglement transitions*, Phys. Rev. B **111**, L060304 (2025), doi:10.1103/PhysRevB.111.L060304.

[28] D. T. Stephen, R. Nandkishore and J.-H. Zhang, *Many-body quantum catalysts for transforming between phases of matter*, PRX Quantum **6**, 020353 (2025), doi:10.1103/PRXQuantum.6.020353.

[29] Y. Zou, S. Sang and T. H. Hsieh, *Channeling quantum criticality*, Phys. Rev. Lett. **130**, 250403 (2023), doi:10.1103/PhysRevLett.130.250403.

[30] Y. Ashida, S. Furukawa and M. Oshikawa, *System-environment entanglement phase transitions*, Phys. Rev. B **110**, 094404 (2024), doi:10.1103/PhysRevB.110.094404.

[31] I. Affleck and A. W. W. Ludwig, *Universal noninteger "ground-state degeneracy" in critical quantum systems*, Phys. Rev. Lett. **67**, 161 (1991), doi:10.1103/PhysRevLett.67.161.

[32] M.-D. Choi, *Completely positive linear maps on complex matrices*, Linear Algebra and its Applications **10**(3), 285 (1975), doi:https://doi.org/10.1016/0024-3795(75)90075-0.

[33] A. Jamiołkowski, *Linear transformations which preserve trace and positive semidefiniteness of operators*, Reports on Mathematical Physics **3**(4), 275 (1972), doi:https://doi.org/10.1016/0034-4877(72)90011-0.

[34] J. Haegeman, K. Van Acoleyen, N. Schuch, J. I. Cirac and F. Verstraete, *Gauging quantum states: From global to local symmetries in many-body systems*, Phys. Rev. X **5**, 011024 (2015), doi:10.1103/PhysRevX.5.011024.

[35] G.-Y. Zhu and G.-M. Zhang, *Gapless coulomb state emerging from a self-dual topological tensor-network state*, Phys. Rev. Lett. **122**, 176401 (2019), doi:10.1103/PhysRevLett.122.176401.

[36] J.-M. Stéphan, S. Furukawa, G. Misguich and V. Pasquier, *Shannon and entanglement entropies of one- and two-dimensional critical wave functions*, Phys. Rev. B **80**, 184421 (2009), doi:10.1103/PhysRevB.80.184421.

[37] J.-M. Stéphan, G. Misguich and V. Pasquier, *Rényi entropy of a line in two-dimensional ising models*, Phys. Rev. B **82**, 125455 (2010), doi:10.1103/PhysRevB.82.125455.

[38] F. C. Alcaraz and M. A. Rajabpour, *Universal behavior of the shannon and rényi mutual information of quantum critical chains*, Phys. Rev. B **90**, 075132 (2014), doi:10.1103/PhysRevB.90.075132.

[39] T. Orito, Y. Kuno and I. Ichinose, *Strong and weak symmetries and their spontaneous symmetry breaking in mixed states emerging from the quantum ising model under multiple decoherence*, URL https://arxiv.org/abs/2412.12738 (2025), 2412.12738.

[40] P. Di Francesco, P. Mathieu and D. Sénéchal, *Conformal field theory*, Graduate Texts in Contemporary Physics. Springer, Germany, ISBN 0-387-94785-X, doi:10.1007/978-1-4612-2256-9 (1997).

[41] M. A. Nielsen and I. L. Chuang, *Quantum Computation and Quantum Information*, Cambridge University Press, USA, 10th edn., ISBN 1107002176 (2011).

[42] C. de Groot, A. Turzillo and N. Schuch, *Symmetry protected topological order in open quantum systems*, Quantum **6**, 856 (2022), doi:10.22331/q-2022-11-10-856.

[43] K. Masuki, H. Sudo, M. Oshikawa and Y. Ashida, *Absence versus presence of dissipative quantum phase transition in josephson junctions*, Phys. Rev. Lett. **129**, 087001 (2022), doi:10.1103/PhysRevLett.129.087001.

[44] J. Y. Lee, Y.-Z. You and C. Xu, *Symmetry protected topological phases under decoherence*, Quantum **9**, 1607 (2025), doi:10.22331/q-2025-01-23-1607.

[45] J. Hauschild and F. Pollmann, *Efficient numerical simulations with Tensor Networks: Tensor Network Python (TeNPy)*, SciPost Phys. Lect. Notes p. 5 (2018), doi:10.21468/SciPostPhysLectNotes.5.

[46] J. Hauschild, J. Unfried, S. Anand, B. Andrews, M. Bintz, U. Borla, S. Divic, M. Drescher, J. Geiger, M. Hefel, K. Hémery, W. Kadow *et al.*, *Tensor network python (tenpy) version 1*, URL https://arxiv.org/abs/2408.02010 (2024), 2408.02010.

[47] In Ref.[19], a fidelity correlator is a better indicator than the Rényi-2 correlator to characterize SWSSBs. However the Rényi-2 correlator still is valid in that it indicates the nontriviality of a state. While the calculation of the fidelity correlator is difficult to be carried out in our numerics, the Rényi-2 correlator is much simpler to calculate than the fidelity correlator and it is compatible in our numerics.

[48] A. Sorge, *autoscale.py - a program for automatic finite-size scaling analyses: A user's guide* (2015).

[49] O. Melchert, *autoscale.py - a program for automatic finite-size scaling analyses: A user's guide*, URL https://arxiv.org/abs/0910.5403 (2009), 0910.5403.

[50] Y. Kuno, S. Sakane, K. Kasamatsu, I. Ichinose and T. Matsui, *Quantum simulation of $(1+1)$-dimensional u(1) gauge-higgs model on a lattice by cold bose gases*, Phys. Rev. D **95**, 094507 (2017), doi:10.1103/PhysRevD.95.094507.

[51] M. Kohmoto, M. den Nijs and L. P. Kadanoff, *Hamiltonian studies of the $d = 2$ ashkin-teller model*, Phys. Rev. B **24**, 5229 (1981), doi:10.1103/PhysRevB.24.5229.

[52] J. Ashkin and E. Teller, *Statistics of two-dimensional lattices with four components*, Phys. Rev. **64**, 178 (1943), doi:10.1103/PhysRev.64.178.

[53] J. Sólyom, *Duality of the block transformation and decimation for quantum spin systems*, Phys. Rev. B **24**, 230 (1981), doi:10.1103/PhysRevB.24.230.

[54] J. B. Kogut, *An introduction to lattice gauge theory and spin systems*, Rev. Mod. Phys. **51**, 659 (1979), doi:10.1103/RevModPhys.51.659.

[55] M. Yamanaka, Y. Hatsugai and M. Kohmoto, *Phase diagram of the ashkin-teller quantum spin chain*, Phys. Rev. B **50**, 559 (1994), doi:10.1103/PhysRevB.50.559.

[56] A. O'Brien, S. D. Bartlett, A. C. Doherty and S. T. Flammia, *Symmetry-respecting real-space renormalization for the quantum ashkin-teller model*, Phys. Rev. E **92**, 042163 (2015), doi:10.1103/PhysRevE.92.042163.

[57] J. C. Bridgeman, A. O'Brien, S. D. Bartlett and A. C. Doherty, *Multiscale entanglement renormalization ansatz for spin chains with continuously varying criticality*, Phys. Rev. B **91**, 165129 (2015), doi:10.1103/PhysRevB.91.165129.